Structure−Activity Relationships for NAMI-A-type Complexes (HL)[*trans*-$RuCl_4L$(*S*-dmso)ruthenate(III)] (L = Imidazole, Indazole, 1,2,4-Triazole, 4-Amino-1,2,4-triazole, and 1-Methyl-1,2,4-triazole): Aquation, Redox Properties, Protein Binding, and Antiproliferative Activity

Michael Groessl, Erwin Reisner, Christian G. Hartinger,*,† Rene Eichinger, Olga Semenova,‡ Andrei R. Timerbaev, Michael A. Jakupec, Vladimir B. Arion, and Bernhard K. Keppler*

Institute of Inorganic Chemistry, University of Vienna, A-1090 Vienna, Austria

Received September 14, 2006

Imidazolium [*trans*-tetrachloro(1*H*-imidazole)(*S*-dimethylsulfoxide)ruthenate(III)] (NAMI-A) and indazolium [*trans*-tetrachlorobis(1*H*-indazole)ruthenate(III)] (KP1019) are the most promising ruthenium complexes for anticancer chemotherapy. In this study, the azole ligand of NAMI-A was systematically varied (from imidazole of NAMI-A to indazole, 1,2,4-triazole, 4-amino-1,2,4-triazole, and 1-methyl-1,2,4-triazole), and the respective complexes were evaluated with regard to the rate of aquation and protein binding, redox potentials, and cytotoxicity by means of capillary zone electrophoresis, electrospray ionization mass spectrometry, cyclic voltammetry, and colorimetric microculture assays. Stability studies demonstrated low stability of the complexes at pH 7.4 and 37 °C and a high reactivity toward proteins (binding rate constants in the ranges of 0.02−0.34 and 0.01−0.26 min^{-1} for albumin and transferrin, respectively). The redox potentials (between 0.25 and 0.35 V) were found to be biologically accessible for activation of the complexes in the tumor, and the indazole-containing compound shows the highest antiproliferative activity in vitro.

Introduction

In the past few years, the interest in anticancer ruthenium(III) compounds, such as imidazolium [*trans*-tetrachloro(1*H*-imidazole)(*S*-dimethylsulfoxide)ruthenate(III)][1] (**1**, NAMI-A, Figure 1) and indazolium [*trans*-tetrachlorobis(1*H*-indazole)-ruthenate(III)][2] (KP1019 or FFC14a, Figure 1), has steadily grown, and both compounds have been the matter of clinical phase I studies.[3,4] In the case of NAMI-A, painful blister formation was considered as dose-limiting toxicity, and the recommended dose of NAMI-A for a phase II study was 300 mg/m^2/day for 5 days every 3 weeks, administered in a 3-h intravenous infusion.[3] On the contrary, administration of KP1019 resulted in comparatively mild side effects and disease stabilizations in the phase I study.[2] The mode of action (Scheme 1) of these potential drugs is supposed to differ from that of the approved platinum-based anticancer agents:[5] NAMI-A and KP1019 are thought to be converted into more active Ru(II) species, facilitating the coordination of a Ru functionality to relevant biomolecules.[6] It is assumed that this reduction process is supported by the reductive environment inside the tumor. Therefore, the knowledge on the electrochemical properties of azole-based ruthenium(III) complexes is of immense importance. Recent research enabled the prediction of the redox potentials of this class of compounds in aqueous medium.[7,8] Additionally, NMR studies revealed that the Ru(III) centers in KP1019[9] and NAMI-A[10] may undergo reduction in the presence of biological reducing agents, e.g., ascorbic acid and glutathione.

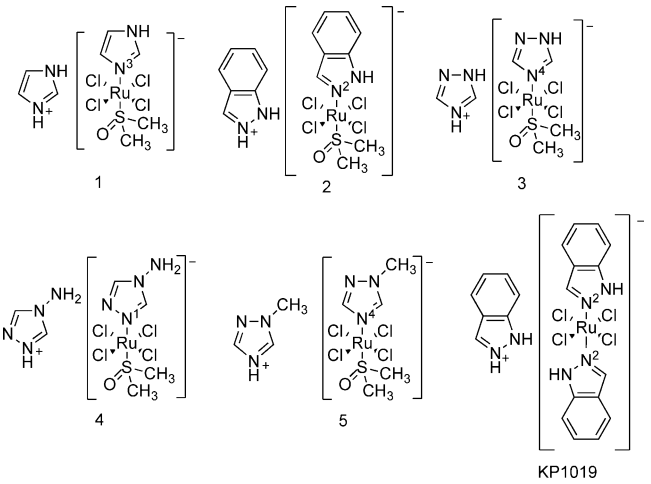

Figure 1. Structural formulas of the studied compounds imidazolium [*trans*-$RuCl_4$(1*H*-imidazole)(dmso-*S*)] (**1**), indazolium [*trans*-$RuCl_4$(1*H*-indazole)(dmso-*S*)] (**2**), 1,2,4-triazolium [*trans*-$RuCl_4$(1*H*-1,2,4-triazole)(dmso-*S*)] (**3**), 4-amino-1,2,4-triazolium [*trans*-$RuCl_4$(4-amino-1,2,4-triazole)(dmso-*S*)] (**4**), and 1-methyl-1,2,4-triazolium [*trans*-$RuCl_4$(1-methyl-1,2,4-triazole)(dmso-*S*)] (**5**), as well as indazolium [*trans*-$RuCl_4$(1*H*-indazole)$_2$] (KP1019).

Scheme 1. Suggested Mode of Action of Ru-Based Anticancer Agents

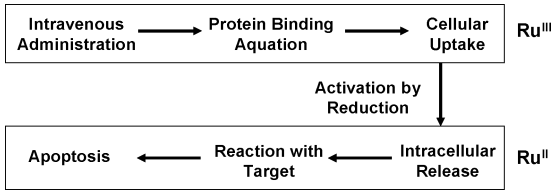

Apart from redox transformations, aquation and interactions with biologically relevant molecules, such as serum transport proteins[11] and DNA nucleotides,[12,13] may play an important role

* To whom correspondence should be addressed. Address: Institute of Inorganic Chemistry, University of Vienna, Waehringer Str. 42, A-1090 Vienna, Austria. Phone: +43 1 4277 52600. Fax: +43 1 4277 9526. E-mail: christian.hartinger@univie.ac.at (C.G.H.); bernhard.keppler@univie.ac.at (B.K.K.).

† Current address: Institut des Sciences et Ingénierie Chimiques, Ecole Polytechnique Fédérale de Lausanne (EPFL), CH-1015 Lausanne, Switzerland.

‡ Current address: Institute of Inorganic Chemistry/Materials Chemistry, University of Vienna, A-1090 Vienna, Austria.

10.1021/jm061081y CCC: $37.00
Published on Web 04/03/2007

in the compounds' mode of action. These processes can be monitored by capillary zone electrophoresis (CZE[a]), which has emerged as an important tool in early stages of metallodrug discovery. Indeed, recent CZE studies provided new facilities for gaining a decent insight into the mode of action of investigational as well as clinically established metal-based anticancer drugs.[14,15] However, no specific information on the drug−protein interaction can be obtained using CZE with conventional UV detection. It is therefore reasonable to combine CZE investigations with electrospray ionization mass spectrometry (ESI-MS[a]) to acquire the stoichiometry of the binding process in a more reliable way. ESI is the softest ionization method available in MS and hence is well-suited for studying the interactions of metal complexes and proteins.[16,17] Specifically, ESI-MS has already found application in the characterization of binding between KP1019 and transferrin.[18]

It is now well-recognized that the interaction with serum proteins takes place immediately after intravenous administration of the ruthenium-based anticancer drugs[19,20] which exhibit yet a stronger affinity toward transferrin and albumin than platinum compounds do.[21] Transferrin, which is mainly responsible for transporting iron through the body to supply the cells, may particularly serve as a natural route for the delivery of the cytotoxic Ru agents to tumor cells as a result of their higher demand for iron.[22,23] Along with transferrin, the most abundant human plasma protein, albumin, displays high binding affinity[21,24] and may contribute to the drug's cellular uptake due to the enhanced permeability and retention (EPR[a]) effect but might also act as a reservoir for the transferrin cycle.

Because of the great promise of NAMI-A as an efficient antimetastatic agent,[1] NAMI-A and its derivatives with different azole ligands were within the focus of the present study. There are extensive research data on the chemical properties[10,25−27] and effects of NAMI-A on the cellular level,[28−33] but its exact mechanism of action still remains obscure. Also, some experimental evidence points out that aquation products, such as polyoxoruthenium species which appear immediately due to the instability of the compound under physiological conditions, are responsible for NAMI-A's selective antimetastatic activity in vivo.[34,35]

To address an issue to a better understanding of the drug's metabolism, the hydrolytic stability of NAMI-A and its derivatives (Figure 1) and the kinetics and stoichiometry of their interaction with human serum albumin and transferrin were explored by CZE and ESI-MS. To elucidate whether the aquation of the compounds of interest affects their protein-binding reactivity, the rate constants of both metabolic processes in physiologically relevant medium were determined and compared. Studies with the aim of ascertaining the cytotoxic efficacies of Ru(III) complexes were performed, and the cytotoxicity data obtained were correlated with pK_a and log P values of the azole ligands. Additionally, redox potentials obtained by cyclic voltammetry were interrelated with the protein binding and cytotoxicity data.

Results and Discussion

To reveal structure−activity relationships (SARs[a]) for NAMI-A-type compounds, more derivatives were synthesized by the reaction of H(dmso)$_2$[*trans*-RuCl$_4$(dmso-*S*)$_2$][36] with an excess of the corresponding azole heterocycle; these derivatives contain 4-amino-1,2,4-triazole and 1-methyl-1,2,4-triazole.[27] Included into the SAR study together with the already known compounds, i.e., (Hind)[*trans*-RuCl$_4$(ind)(dmso-*S*)], (Him)[*trans*-RuCl$_4$(im)(dmso-*S*)], and (Htrz)[*trans*-RuCl$_4$(trz)(dmso-*S*)], these allowed us to compare the pharmacologically essential properties with different pK_a values of the azole ligands. Note that the latter structure-dependent parameter has a direct impact on the redox properties of this family of compounds.[7] Furthermore, for structural characterization of the metal-complex anions, single crystals of the corresponding (Ph_3PCH_2Ph) complex salts of the atrz- and mtrz-containing compounds suitable for X-ray diffraction study were obtained by a decelerated metathesis of (HL)[*trans*-RuCl$_4$L(dmso-*S*)] and (Ph_3PCH_2Ph)Cl (see Supporting Information).

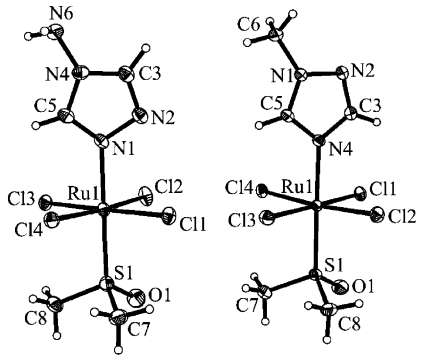

Figure 2. Structure of [*trans*-RuCl$_4$(atrz)(dmso-*S*)]$^-$ in **4a**·H$_2$O (left) and [*trans*-RuCl$_4$(mtrz)(dmso-*S*)]$^-$ in **5a** (right) showing the atom-numbering scheme. Thermal displacement ellipsoids are drawn at the 50% probability level.

Crystal Structures of 4a·H$_2$O and 5a. Different azole ligands and different coordination modes are known to have an effect on the antiproliferative activity of ruthenium(III) complexes.[37] 1,2,4-Triazole ligands are particularly interesting, because they are recognized as adopting a variety of coordination modes,[38] which have been clarified by X-ray crystallography. Both monodentate coordination via *N*4 or the less basic *N*2 coordination of unsubstituted 1,2,4-triazole to ruthenium(III) have been reported for ruthenium(III) complexes.[7,37] 1,2,4-Triazole in (PPN)[*trans*-RuCl$_4$(trz)(dmso-*S*)] (PPN = bis(triphenylphosphine)iminium chloride[a]) was shown to coordinate via *N*4.

The coordination of the 1,2,4-triazole ligand in compounds **4** and **5** is controlled by the substitution site of 1,2,4-triazole. The use of 1-methyl-1,2,4-triazole was expected to result in coordination via *N*4, while for 4-amino-1,2,4-triazole, coordination via *N*1 was supposed. This was confirmed for (Ph_3PCH_2-Ph)[*trans*-RuCl$_4$(atrz)(dmso-*S*)] and (Ph_3PCH_2Ph)[*trans*-RuCl$_4$-(dmso-*S*)(mtrz)] (both shown in Figure 2) by X-ray diffraction analysis.

The complexes containing a ruthenium(III) central atom have a distorted octahedral geometry with four chloro ligands in the equatorial positions and a dmso molecule bound via its sulfur atom trans to the azole ligand in the axial position. The bond lengths and angles are comparable to those found in other NAMI-A derivatives.[39,40] Selected bond lengths and angles are quoted in Table 1, whereas crystallographic data for **4**·H$_2$O and **5** are included in the Supporting Information.

Cyclic Voltammetry. The redox behavior of **1** in aqueous solution was reported previously by Osella et al.[8] In our experiments, all tested compounds exhibited reduction potentials similar to that of **1** at neutral pH, and CVs of compounds **1**−**5**

[a] Abbreviations: atrz, 4-amino-1,2,4-triazole; BGE, background electrolyte; CV, cyclic voltammogram; CZE, capillary zone electrophoresis; dmso, dimethyl sulfoxide; EPR, enhanced permeability and retention; ESI, electrospray ionization; IC$_{50}$, 50% inhibitory concentration; im, 1*H*-imidazole; ind, 1*H*-indazole; MS, mass spectrometry; mtrz, 1-methyl-1,2,4-triazole; MTT, 3-(4,5-dimethylthiazol-2-yl)-2,5-diphenyltetrazolium bromide; NHE, normal hydrogen electrode; PPN, bis(triphenylphosphine)iminium chloride; SAR, structure−activity relationship; trz, 1*H*-1,2,4-triazole.

Table 1. Selected Bond Lengths (Å) and Angles (deg) in the Coordination Polyhedron of **4a**·H_2O and **5a**

	4a·H_2O	**5a**
atom1−atom2		
Ru1−N	2.0910(14)	2.0935(18)
Ru1−S1	2.2906(6)	2.2776(10)
Ru1−Cl1	2.3565(5)	2.3364(7)
Ru1−Cl2	2.3409(5)	2.3424(9)
Ru1−Cl3	2.3535(5)	2.3618(9)
Ru1−Cl4	2.3727(5)	2.3805(7)
atom1−atom2−atom3		
N−Ru1−S1	177.35(4)	179.14(5)

Table 2. Summary of Structural and Activity Parameters of Ruthenium(III) Complexes

	compd **1** (im)	compd **2** (ind)	compd **3** (trz)	compd **4** (atrz)	compd **5** (mtrz)
$\tau_{1/2}$ (min)					
aquation[a]	20.6 ± 1.4	24.4 ± 1.0	23.2 ± 2.3	9.5 ± 0.3	27.5 ± 1.4
albumin[a]	9.2 ± 0.5	7.1 ± 0.5	9.2 ± 0.8	5.8 ± 0.2	13.8 ± 1.1
transferrin[a]	14.5 ± 0.6	8.9 ± 0.4	11.9 ± 0.8	6.1 ± 0.2	17.7 ± 1.4
$E_{1/2}$ (V)	0.25	0.35	0.30	0.28	0.29
IC_{50}[b] (μM)					
HT-29	339 ± 68	212 ± 22	322 ± 32	621 ± 5	315 ± 22
SK-BR-3	472 ± 25	169 ± 10	415 ± 48	>1000	517 ± 70
log P_{azole}[c]	−0.25	1.47	−0.44	−2.11	−0.49
p$K_{a,N-Ru}$[d]	6.99	1.04	2.45	3.20	3.23

[a] Half-life values correspond to the time when the peak area of the monitored complex is reduced to 50% of the initial value. For conditions see Materials and Methods. [b] 50% inhibitory concentrations in the MTT assay (exposure time, 96 h). Values are the means ± standard deviations obtained from at least three independent experiments. [c] log *P* values of the azole ligands were calculated using: *MarvinSketch 4.0.6*; ChemAxon: Budapest, Hungary, 1998−2006; http://www.chemaxon.com/marvin. [d] pK_a values correspond to the coordinating nitrogen atoms of the azole ligands.[56]

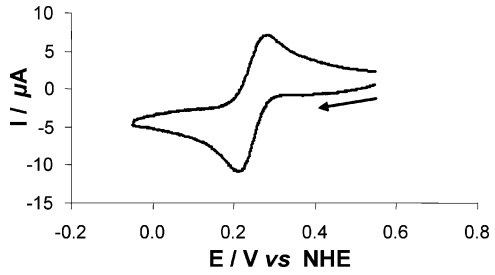

Figure 3. Cyclic voltammogram of 4 mM **5** in 0.20 M phosphate buffer (pH 7.0) at a glassy carbon working electrode and at a scan rate of 10 mV/s showing the Ru^{III}/Ru^{II} redox couple.

displayed one reversible Ru^{III}/Ru^{II} reduction wave in 0.20 M phosphate buffer at pH 7.0 (Figure 3; only the CV of **5** is included for the sake of conciseness). The redox potentials were measured as 0.25, 0.35, 0.30, 0.28, and 0.29 V vs NHE for **1**−**5**, respectively, thus substantiating an expected tendency: the lower the basicity of the coordinated azole ligand, the higher is the $E_{1/2}$ of the complex (see Table 2). It is worth mentioning that the assessed redox potentials fall in the biologically relevant and accessible range; in proliferating cells, the reduction potential is about −0.24 V vs NHE,[41] while inside the tumor it is up to 100 mV lower.[42] This means that biological reducing agents, e.g., glutathione or ascorbic acid, are capable of reducing the compounds to the corresponding Ru(II) species, as already reported for **1**.[8]

Capillary Zone Electrophoresis. (a) Stability. CZE has frequently been utilized for the monitoring of the aquation of pharmaceutically relevant metal complexes.[15] For example, Timerbaev et al. described the hydrolytic behavior of KP1019 (and also its binding to serum transport proteins),[21] and the hydrolytic metabolite of cisplatin in human serum was quantified

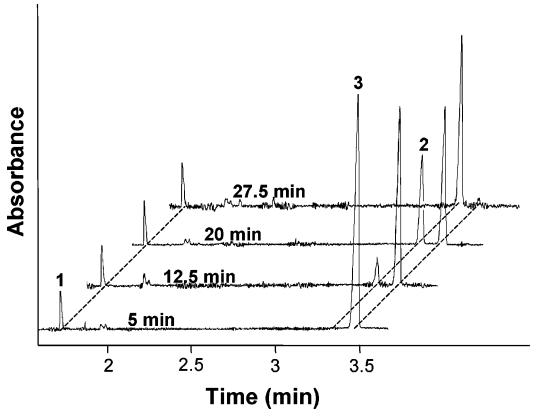

Figure 4. Monitoring of the aquation reaction of compound **1** by CZE: sample concentration, 1 mM; separation voltage, 20 kV. Other conditions: see Materials and Methods. Peak identification: 1, imidazolium; 2, aquation product; 3, [*trans*-$RuCl_4$(1*H*-imidazole)(dmso-*S*)]$^-$.

by Huang et al.[43] Stability in aqueous solution constitutes an essential requirement for pharmaceutical preparations,[44] whereas binding to proteins after intravenous administration is considered as an important metabolic step in the mode of action of Ru(III)-based anticancer agents. Nevertheless, in blood there are yet a number of competitive reactions likely to occur within the time scale of (rather fast) protein binding processes, e.g., reduction by cysteine or glutathione or hydrolytic substitution of chloro ligands. Importantly, hydrolysis products of NAMI-A are even thought to be responsible for the drug's selective inhibition process of metastasis in vivo.

Figure 4 shows a series of electropherograms depicting the aquation of NAMI-A in the incubation solution (that proceeds via replacement of chloro ligands by aqua ligands) recorded for comparative purposes at different time. These two processes can be followed by the decline of the [*trans*-$RuCl_4$(im)(dmso-*S*)]$^-$ peak area and the increase in the area of the peak assigned to the aquation product (peak 2), respectively. After reaching a maximum value, the latter signal, however, tends to decrease apparently due to further hydrolysis. The possibility of Anderson rearrangement,[45] implying dehalogenation caused by the replacement of inner chloride ligand(s) by outer-sphere azole ligand(s), was ruled out by spiking the solution with the corresponding complex. For all compounds tested, a comparable character of changes in the hydrolysis-related electrophoretic profiles was observed; that is, the complex anion peak area falls beyond 50% of its initial value in less than 30 min, followed by the disappearance of the peak due to the aquation within 100 min. Notably, hydrolysis caused a gradual darkening of the sample solutions, presumably due to the formation of insoluble μ-oxo-bridged polyruthenium species. The formation of such polymeric forms was proposed in recent NMR studies for NAMI-A,[1,11,35] as a result of a stepwise loss of the chloro ligands and the following partial release of the dmso ligand.

The time dependences of the normalized peak areas for the intact ruthenium complexes, presented in Figure 5, demonstrate that initially aquation progresses rather slowly but is then accelerated by the formation of the aquation product. For the compounds with unsubstituted azole ligands, i.e., **1**−**3**, half-lives of about 20 min were found. In contrast, the substituted azole complexes behave quite differently: While the aminotriazole-containing compound **4** shows much faster aquation than all the other complexes, the methyltriazole derivative **5** is the complex with the lowest aquation rate. Methylation of the triazole ligand might lead to a stabilization of the Ru−Cl bond.

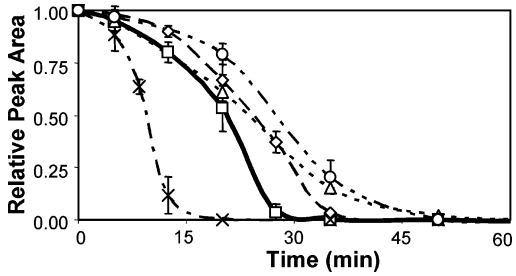

Figure 5. Time courses of the aquation reaction for [*trans*-$RuCl_4$(im)(dmso-*S*)]$^-$ (-□-), [*trans*-$RuCl_4$(ind)(dmso-*S*)]$^-$ (-◇-), [*trans*-$RuCl_4$(trz)(dmso-*S*)]$^-$ (-△-), [*trans*-$RuCl_4$(atrz)(dmso-*S*)]$^-$ (-×-), and [*trans*-$RuCl_4$(mtrz)(dmso-*S*)]$^-$ (-○-). The error bars represent the standard deviations.

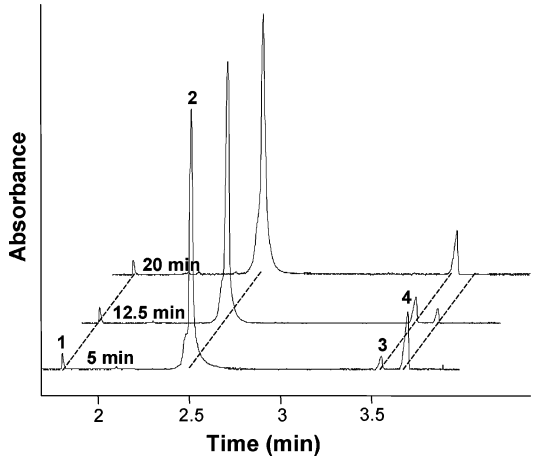

Figure 6. Monitoring of the interaction of compound **1** with transferrin. Peak identification: 1, imidazolium; 2, Ru−protein adduct and free transferrin; 3, aquation product; 4, [*trans*-$RuCl_4$(im)(dmso-*S*)]$^-$. Conditions: see Figure 4.

The observed influence of the aminotriazole ligand is in accord with previous results on the effect of introducing an amino group into the nitrogen heterocyclic ligand of KP1019-analogous complexes.[46] Note that the indazole derivative **2** was the most stable Ru(III) complex under scrutiny. In the case of the 1,2,4-triazole derivative **3**, the interpretation of the electropherograms was complicated by the fact that some additional partially resolved peaks were observed, probably attributable to isomeric species.

(b) Protein Binding. The binding kinetics for the reactions of NAMI-A and analogous compounds with albumin and transferrin were characterized by CZE. A series of papers dealing with the interaction of NAMI-A with pertinent biomolecules in vitro and in vivo have been published using various analytical methods.[29,34,47] Favorably, the use of CZE renders several advantages regarding simultaneous characterization of the constituents of interest in the (complex) sample mixture based on the technique's excellent separation ability and short analysis time. Electropherograms illustrating the interaction with human serum albumin (data not shown) and transferrin (Figure 6) were recorded at different incubation times. Similarly to aquation studies, the problem of overlapping peaks was again faced with the triazole complex **3**; however, this did not hinder appropriate data interpretation. The results confirm that in the case of both proteins binding occurs rapidly, as indicated by a faster disappearance of the peaks of the unbound complex and by shorter half-lives of Ru compounds than in the case of hydrolytic decomposition. A significant change in the rate constants (cf. k_{aqua} and $k_{aqua+bind}$ data sets shown in Table 3) underlines this finding, with the k values increasing caused by the presence of serum proteins. A closer look at the constants also reveals that binding to albumin is kinetically slightly favored over transferrin binding, as also evidenced from comparison of the graphic depiction of binding kinetics (Figure 7).

When comparing the curves and rate constants of the hydrolytic decomposition reactions to those describing the binding to the proteins, it is obvious that the complex anions react more rapidly in the presence of the biomolecules. Among the Ru complexes examined, compound **2** exhibits the fastest binding to the proteins in contrast to its slow rate of aquation, indicating a strong influence of the indazole group on the drug−protein interaction. From the clinical point of view, this suggests that complex **2** would advantageously be converted into the protein-bound form faster than the other complexes, considering the importance of the transport of transferrin conjugates via the transferrin receptor route, as well as the EPR effect in the case of albumin adducts. One can speculate that aquation facilitates the interaction with proteins since the peak area corresponding to the hydrolysis product likewise decreases at a faster rate when analyzing the protein-containing samples. Control experiments conducted with compound **1** showed that the addition of 100 mM NaCl to the incubation solution greatly decelerates the exchange of the chloro ligands with water; the peak belonging to the aqua species did not appear after more than 3 h of incubation. Still, binding to albumin was only decelerated by a factor of 2 under these conditions. This implies that while the hydrolytic transformation may bring about an accelerated binding to the proteins, it seems not to be a prerequisite for protein binding. Apparently, proteins catalyze the formation of aqua species (cf. kinetic data for compound **1**, Figure 7). Consequently, for all studied compounds the rate constants of transformation are considerably higher (and the half-lives shorter) in the presence of albumin or transferrin as compared to the aquation process (see Tables 2 and 3). The differences in the behavior of the triazole-containing complexes are prominent as well: The presence of the primary amine group (which allows hydrogen bonding toward electron-acceptor protein residues) in **4** accelerates the protein−complex conjugation, whereas the methyl group has an opposite, inhibiting effect. The half-life of the unsubstituted triazole complex **3** (intermediate $\tau_{1/2}$ of **4** and **5**) suggests less pronounced hydrogen-bonding interactions.

It should be emphasized that the modeling of kinetic and equilibrium processes of metal complexes in biochemical systems can only be based on hypothesized reaction mechanisms—even stoichiometrically simple reactions consist of many elementary steps. Real-world samples in general comprise a great complexity resulting from numerous metabolic transformations and frequent ligand-exchange reactions with different biological molecules. Therefore, for the estimation of the rate constants, a hypothesized pseudo-first-order reaction mechanism was considered, and for the calculation of the rate constants only the linear range of the curves was taken. Thus, hypothetical extrapolation of linear curves according to the linear equation used for the estimations of pseudo rate constants (Table 3) can result in half-lives different from those determined from the experimental curves (Table 2).

Mass Spectrometry. For determination of the stoichiometry of the protein adducts, ESI-MS experiments were performed. Since signal suppression is observed in ESI-MS of phosphate buffer solutions, 20 mM ammonium bicarbonate buffer at physiological pH was utilized. Although ESI is considered the softest ionization method, metal complexes frequently undergo

Table 3. Summary of Rate Constants[a] for Metabolically Important Transformations of the Studied Ruthenium Compounds

		k_{bind}[c] (min^{-1})		$k_{aqua+bind}$ (min^{-1})	
compound	k_{aqua} (min^{-1})	albumin	transferrin	albumin	transferrin
1 (im)	0.031 ± 0.006 (0.931)[b]	0.166 ± 0.044 (0.919)	0.064 ± 0.024 (0.874)	0.099 ± 0.025 (0.907)	0.047 ± 0.015 (0.818)
2 (ind)	0.020 ± 0.005 (0.907)	0.282 ± 0.051 (0.929)	0.206 ± 0.027 (0.935)	0.151 ± 0.028 (0.951)	0.113 ± 0.016 (0.962)
3 (trz)	0.025 ± 0.004 (0.965)	0.123 ± 0.036 (0.936)	0.094 ± 0.014 (0.961)	0.074 ± 0.020 (0.907)	0.060 ± 0.009 (0.957)
4 (atrz)	0.050 ± 0.012 (0.943)	0.344 ± 0.092 (0.914)	0.258 ± 0.054 (0.940)	0.197 ± 0.052 (0.884)	0.154 ± 0.033 (0.936)
5 (mtrz)	0.012 ± 0.002 (0.977)	0.021 ± 0.006 (0.956)	0.009 ± 0.003 (0.960)	0.016 ± 0.004 (0.935)	0.010 ± 0.002 (0.943)

[a] For conditions see Materials and Methods. [b] Given in parentheses is the correlation coefficient (R) for the corresponding rate equation. [c] Calculated as the difference between k values of summation and hydrolytic processes (see Materials and Methods).

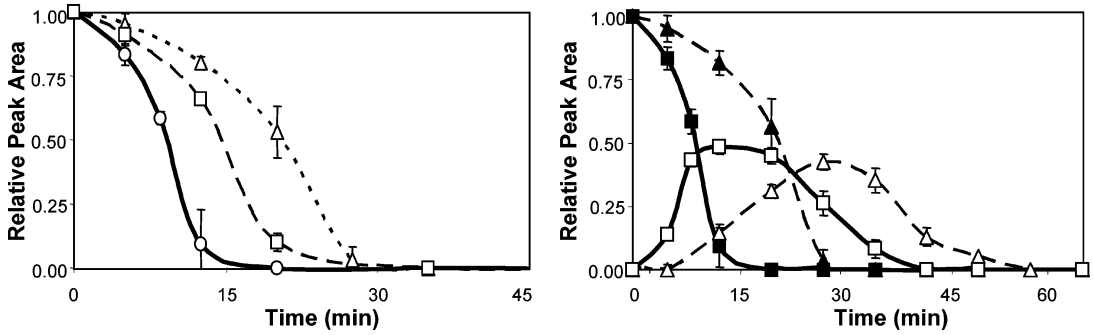

Figure 7. Aquation and protein binding kinetics of **1** (NAMI-A). Left: Decrease of the complex peak area in the presence of albumin (-○-) and transferrin (-□-) and due to hydrolytic decomposition only (-△-). Right: Monitoring of the peak areas of NAMI-A and the corresponding aqua species in phosphate buffer solution without (-▲- and -△-, respectively) and in the presence of albumin (-■- and -□-).

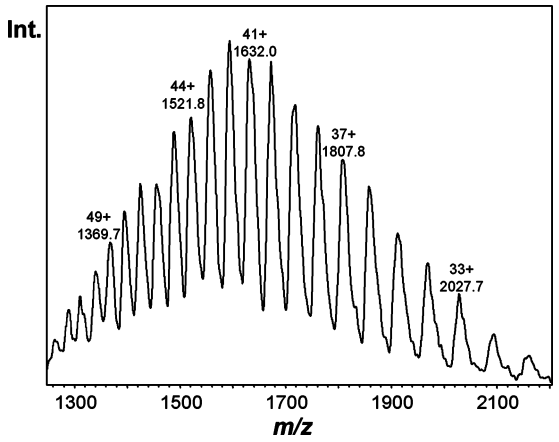

Figure 8. Mass spectrum of a conjugate formed by [*trans*-$RuCl_4$(trz)-(dmso-*S*)]$^-$ after incubation of human serum albumin with compound **3** at 1:1 ratio. A mass increase of approximately 400 Da corresponding to the addition of a single complex anion can be observed. For measurement parameters see Materials and Methods.

fragmentation processes.[48,49] Still, many examples of the successful application of ESI-MS for the analysis of metal−protein adducts have been reported.[18]

For comparative purposes, solutions containing only the proteins were prepared to assess their molecular weights; charge deconvolution yielded an average molecular mass of 66 645 ± 36 Da for albumin (spectrum not shown). This is slightly higher than the reported mass of 66 478 Da and might be caused by alkali metal adduct formation, disulfide formation at Cys-34, and/or different glycosylation of the protein specimens.[50] After 30 min of incubation with the ruthenium(III) complexes, main peaks could be attributed to adducts formed between one to two complex anions and the protein (Figure 8), the number of adducts depending on the drug-to-protein ratio. Due to very strong interfering effects of unbound Ru compounds at drug-to-protein ratios of 20:1, it was only possible to carry out experiments with ratios up to 10:1. Additional peaks presumably originate from binding of hydrolysis products. Referring to the literature, it has been proposed that only 1 equiv of NAMI-A binds specifically to the protein, namely, to one of the histidine residues.[51] In addition, up to four unspecifically bound Ru residues are scattered over the surface of the molecule, some of which might be removed after spraying and ionization. Therefore, the acquired stoichiometric results are overall in accord with the literature data. To ensure equilibrium conditions, the measurements were repeated after an incubation period of 180 min, yielding essentially the same results.

In the case of transferrin, an average molecular mass of 79 635 ± 37 Da was determined (spectrum not shown), which is also slightly higher than the reported one of 79 557 Da.[50] The ESI mass spectrum of compound **3** bound to transferrin is shown in Figure 9. Because of the mass inaccuracy of a mass spectrometer equipped with an ion trap analyzer, the exact structure of the adduct cannot be elucidated and would require analysis with an instrument of higher resolution. Additionally, due to the broad isotopic pattern of ruthenium complexes, especially those with chloro ligands, and the low resolution of the instrument, the protein conjugates formed do not show sharp but rather broad and overlapping peaks, especially at high drug-to-protein ratios. Nonetheless, it was possible to confirm for all the compounds by a mass increase of ca. 400 Da that at least one Ru moiety per protein molecule was bound at all drug-to-protein ratios studied. Consequently, the mass increase of approximately 800 Da was assigned to the formation of bisadducts.

Cytotoxicity. The cytotoxic potencies of compounds **1**−**5** were investigated in two human tumor cell lines HT-29 (colon carcinoma) and SK-BR-3 (mammary carcinoma) by means of the colorimetric MTT assay. Concentration−effect curves are

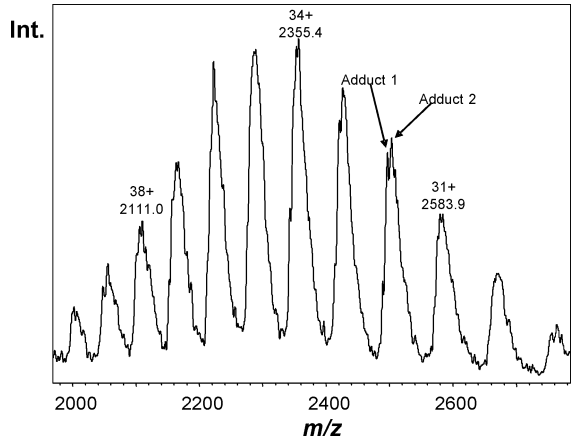

Figure 9. Mass spectrum of a conjugate formed by transferrin with [*trans*-$RuCl_4$(mtrz)(dmso-*S*)]$^-$ after incubation at a drug-to-protein ratio of 2:1. The labeled peaks correspond to an adduct formed by the addition of a single complex molecule; the mass difference between the protein itself and the conjugate was approximately 400 Da (adduct 1). A second conjugate can also be identified with a mass difference of approximately 800 Da (adduct 2) formed by the addition of a second complex molecule. For measurement parameters see Materials and Methods.

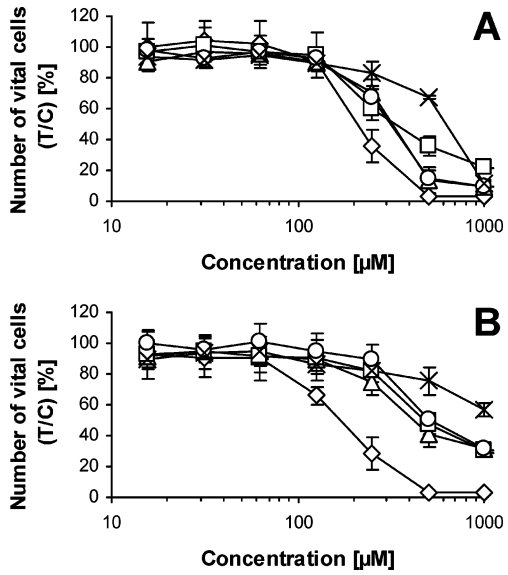

Figure 10. Concentration−effect curves of ruthenium(III) complexes of the general formula (HL)[*trans*-$RuCl_4$(azole)(dmso-*S*)] (L = azole ligand): **1** (im) (-□-), **2** (ind) (-◇-), **3** (trz) (-△-), **4** (atrz) (-×-), and **5** (mtrz) (-○-), obtained by the MTT assay in (A) HT-29 cells and (B) SK-BR-3 cells. Values are means ± standard deviations from at least three independent experiments.

depicted in Figure 10, and IC_{50} values are listed in Table 2. Generally, SK-BR-3 cells are less sensitive to the test compounds, with the exception of **2**. The cytotoxicities of the complexes are rather moderate, with IC_{50} values ranging between 210 and 620 μM in HT-29 cells and between 170 and >1000 μM in SK-BR-3 cells. Only in the case of **4**, the IC_{50} could not be reached in SK-BR-3 cells. With respect to the *N*-heterocyclic ligand, the cytotoxicity of the complexes decreases in the following order: **2** (ind) > **3** (trz) ≈ **5** (mtrz) ≈ **1** (im) > **4** (atrz).

SARs. By relating the pK_a values of the azole ligands, the protein binding, and cyclic voltammetric data of compounds **1**−**3** with the substances' IC_{50} values (see Table 2), certain SARs were observed. In particular, **2** was found to display the highest reactivity toward the proteins, and it was also the most cytotoxic complex while the rate of aquation for **1**−**3** was within the same dimension. A higher basicity of the azole ligand was also reflected by a lower Ru^{III}/Ru^{II} redox potential of the respective complexes. Furthermore, it seems that, similarly to complexes of the general formula (Hazole)[*trans*-$RuCl_4$(azole)$_2$], the indazole ligand has a favorable effect on the protein-binding kinetics. Interestingly, complexes **4** and **5**, containing the substituted triazole ligands, do not follow this tendency. This is indicative of a strong influence of both the amino and methyl group on the molecular stability and reactivity toward proteins, probably as a result of the formation of hydrogen bonds to protein side chains of **4**. Notably, the introduction of the methyl group leads, in comparison to NAMI-A and the trz derivative **3**, to a more stable compound with similar in vitro activity that might be explained by an increased uptake into the cell due to a higher lipophilicity. Interestingly, comparison of the cytotoxicity tests with results reported for (Hind)[*trans*-$RuCl_4$(ind)$_2$] and its structural analogue imidazolium [*trans*-tetrachlorobis(1*H*-imidazole)ruthenate(III)] (KP418)[52,53] confirms that indazole-containing complexes exhibit higher activity than those with imidazole ligands.

Turning to the analysis of relevant pharmacological properties evaluated in this study, in terms of quantitative SARs, consistent approximations for the whole set of complexes were only obtained between IC_{50} and log *P* values, i.e., $R = 0.927$ and 0.962 for HT-29 and SK-BR-3, respectively. This means that the compounds with higher lipophilicity (within the thresholds shown in Table 2) turn out to exhibit higher in vitro cytotoxicity, presumably as a result of higher cellular bioavailability.

Conclusions

Ruthenium(III) complexes are among the most intensively studied alternatives to platinum compounds in cancer chemotherapy. Aquation, protein binding, and activation by reduction are regarded as important steps with respect to their mode of action. In the present study, NAMI-A was compared to a representative number of analogous compounds with varying azole ligands in terms of stability in aqueous solution, interaction with the most important plasma proteins, redox potentials, and antiproliferative activity. It was shown that in phosphate buffer (pH 7.4) at 37 °C all compounds exhibit hydrolytic stabilities with half-lives of less than 30 min. As already applied for NAMI-A administration, a suitable formulation for all these compounds should contain a physiological concentration of NaCl to enhance the stability in the infusion solution (which is more than 3 h for the parent drug[3]). Aquation does not seem to influence the rate of protein binding of the compounds, and in general binding to albumin appears to be kinetically favored over that to transferrin, with **2** (ind) and **4** (atrz) being the most reactive representatives. However, no specific binding information could be gained using CZE with UV-absorbance detection. Future studies will, therefore, be focused on online coupling of CZE to an ESI-MS or an element-specific inductively coupled plasma-MS detector for structural and functional characterization of the ruthenium−protein adducts.

Cytotoxicity investigations in cancer cell lines revealed similar IC_{50} values for complexes **1**, **3**, and **5**, while compounds **2** and **4** were significantly more and less active, respectively. For compounds **1**−**3**, dependencies between the redox potentials, pK_a values of the azole ligands, protein-binding rate constants, and IC_{50} values were found: lower pK_a of the azoles results in larger $E_{1/2}$ of the corresponding ruthenium complexes and higher antitumor activity. Furthermore, faster protein binding was associated with higher antineoplastic potency. Surprisingly,

comparison of the different triazole-containing complexes in terms of antiproliferative activities showed that the aminotriazole complex **4** is the least active of all tested compounds, albeit it has the highest reactivity toward the serum proteins. The amino substituent might not only favor the formation of hydrogen bonds with protein side chains but also lower the complex's antineoplastic potency, whereas the methyl substituent does not seem to alter the substance's activity. This shows that assumed advantages due to marked protein binding properties are offset by a lack of stability, probably resulting in unspecific reactions.

Since NAMI-A has a proven antimetastatic potency, in vivo studies may enlighten the potential of its derivatives as drug candidates. Yet before these trials, a hit compound identification program should be implemented widely for this compound family as based on SARs demonstrated here. Careful selection and chemical modification of the azole ligands might allow the respective complexes' properties to be efficiently tuned with regard to inertness, rate of protein binding, and cytotoxic activity.

Materials and Methods

Chemicals. Sodium hydroxide and sodium dihydrogenphosphate were obtained from Fluka (Buchs, Switzerland). Disodium monohydrogenphosphate was purchased from Riedel-de Haen (Seelze, Germany). Human serum albumin (approximately 99%, Lot 111K7612), apo-transferrin (≥97%, Lot 074K1370), and ammonium bicarbonate (purum, p.a.) were the products of Sigma-Aldrich (Vienna, Austria). Transferrin and albumin concentrations were determined spectrophotometrically from the molar absorptivities of 8.38×10^4 and 4.08×10^4 cm^{-1} M^{-1} at 280 nm for the two proteins, respectively.[52] High-purity water used throughout this work was obtained from a Millipore Synergy 185 UV Ultrapure Water system (Molsheim, France). 4-Amino-1,2,4-triazole (atrz[a]) and 1-methyl-1,2,4-triazole (mtrz[a]) were obtained from Fluka and Lancaster (Karlsruhe, Germany), respectively, and used without further purification.

Preparation and Characterization of Ruthenium Complexes. H(dmso)$_2$[*trans*-RuCl$_4$(dmso-*S*)$_2$],[47] (Him)[*trans*-RuCl$_4$(im)(dmso-*S*)] (**1**, NAMI-A),[54] (Hind)[*trans*-RuCl$_4$(ind)(dmso-*S*)] (**2**),[7] and (Htrz)[*trans*-RuCl$_4$(trz)(dmso-*S*)] (**3**)[7] (where im = 1*H*-imidazole,[a] ind = 1*H*-indazole,[a] trz = 1*H*-1,2,4-triazole,[a] and dmso = dimethylsulfoxide[a]) were prepared as described elsewhere.

Synthesis of (Hatrz)[*trans*-RuCl$_4$(atrz)(dmso-*S*)] (4). Atrz (0.20 g, 2.4 mmol) was dissolved in methanol (1 mL), and the resulting solution was added dropwise to a solution of H(dmso)$_2$[*trans*-RuCl$_4$(dmso-*S*)$_2$] (0.20 g, 0.36 mmol) in 5 mL of methanol. The mixture was vigorously stirred for 1.5 h, whereupon the yellow precipitate formed was filtered off, washed with ethanol, diethyl ether, and dried under vacuum at room temperature. Yield: 0.12 g, 68%. Anal. ($C_6H_{15}N_8Cl_4ORuS$): C, H, N, Cl, S. ESI-MS (negative), *m*/*z* 406 [RuCl$_4$(atrz)(dmso-*S*)]$^-$, 322 [RuCl$_4$(dmso-*S*)]$^-$, 244 [RuCl$_4$]$^-$. ESI-MS (positive), *m*/*z* 85, [Hatrz]$^+$. UV−vis (H_2O), λ_{max}, nm (ϵ, M^{-1} cm^{-1}): 461 (538), 397 (3950), 292 (1332). Crystals suitable for X-ray diffraction study were grown in an H-shaped tube by a slowed down metathesis reaction between (Hatrz)[*trans*-RuCl$_4$(atrz)(dmso-*S*)] and (Ph_3PCH_2Ph)Cl in aqueous ethanol, yielding (Ph_3PCH_2Ph)[*trans*-RuCl$_4$(atrz)(dmso-*S*)]·H_2O (**4a**·H_2O) (see Supporting Information).

Synthesis of (Hmtrz)[*trans*-RuCl$_4$(mtrz)(dmso-*S*)] (5). Mtrz (0.10 mL, 2.4 mmol) was added to a solution of H(dmso)$_2$[*trans*-RuCl$_4$(dmso-*S*)$_2$] (0.10 g, 0.18 mmol) in ethanol (96%, 2 mL). The reaction mixture was then stirred and the precipitation of the product initiated by grinding with a glass stick on the glass surface of the round-bottomed flask. The yellow precipitate was filtered off after 1 h, washed with ethanol and diethyl ether, and dried under vacuum at room temperature. Yield: 0.06 g, 63%. Anal. ($C_8H_{17}N_6Cl_4ORuS$): C, H, N, Cl, S. ESI-MS (negative), *m*/*z* 405 [RuCl$_4$(dmso-*S*)(mtrz)]$^-$, 322 [RuCl$_4$(dmso-*S*)]$^-$, 244 [RuCl$_4$]$^-$. ESI-MS (positive), *m*/*z* 84, [Hmtrz]$^+$. UV−vis (H_2O), λ_{max}, nm (ϵ, M^{-1} cm^{-1}): 459 (501), 395 (4066), 292 (1328). Crystals suitable for X-ray diffraction study were grown in an H-shaped tube by a slowed down metathesis reaction between (Hmtrz)[*trans*-RuCl$_4$(mtrz)(dmso-*S*)] and (Ph_3PCH_2Ph)Cl in aqueous ethanol, yielding (Ph_3PCH_2Ph)[*trans*-RuCl$_4$(mtrz)(dmso-*S*)] (**5a**) (see Supporting Information).

Electrochemical Studies. Cyclic voltammograms (CVs[a]) were measured in a three-electrode cell equipped with a 0.2-mm-diameter glassy carbon working electrode, a platinum auxiliary electrode, and an Ag|AgCl reference electrode, and filled with 0.20 M phosphate buffer. Measurements were performed using an EG&G PARC 273A potentiostat/galvanostat (Oak Ridge, TN) at room temperature. Deaeration of solutions was accomplished by passing a stream of argon for 5 min before the measurement and maintaining a blanket atmosphere of argon over the measured solution during the analysis. The redox potentials are quoted relative to the normal hydrogen electrode (NHE[a]).

Samples and Electrolytes. A 20 mM phosphate buffer (pH 7.4) was chosen as incubation buffer and background electrolyte (BGE[a]) for the electrophoretic separations. The BGE was passed through a 0.45 μm disposable membrane filter (Sartorius, Goettingen, Germany) before CZE analysis. The initial protein and ruthenium complex concentrations in the sample mixtures were fixed at 50 μM and 1 mM, respectively, in 20 mM phosphate buffer (pH 7.4) incubated at 37 °C. This constitutes a protein-to-drug ratio of 1:20, which is a reasonable approximation of a real situation at the first steps after intravenous administration.

Capillary Zone Electrophoresis. CZE experiments were performed with an HP^{3D} CE system (Agilent, Waldbronn, Germany) equipped with a diode-array detector. For all measurements, uncoated fused silica capillaries of 50 cm total length (50 μm i.d., 42 cm effective length) were used (Polymicro Technologies, Phoenix, AZ). Capillary and sample tray were thermostatted at 37 °C. Injections were performed by applying a pressure of 50 mbar for 3 s, and a constant voltage of 20 kV was used for all separations (the resulting current was about 35 μA). Detection was carried out at 200 nm. Prior to a first use, the capillary was flushed with 0.1 M HCl, water, 1 M NaOH, and again with water (10 min each) and then equilibrated with the BGE for 10 min. Before each injection, the capillary was purged with 0.1 M NaOH and water for 2 min each and finally conditioned with the BGE for 3 min.

The rate of hydrolytic and protein-binding reactions was measured by monitoring the decrease of the peak area response due to the Ru-complex anions. All rates were determined in 20 mM phosphate buffer (pH 7.4) at 37 °C; the sample solutions were prepared as described above, the resulting ion strength was about 52 mmol/L. The peak areas were normalized with respect to the area of the peak of the respective counterion. For the determination of the rate constants (k_{aqua} and $k_{aqua+bind}$, respectively), each kinetic series was repeated at least three times on the same working day. It should be noted that the kinetics of Ru−protein binding was assessed indirectly because the peak of the adduct could not be separated from the protein peak or selectively recorded using the UV detection mode. Apparent binding rate constants were calculated by polynomial approximation of the rate constants of both processes, assuming the first-order character of the binding reaction. In accordance with the theory of two parallel reactions kinetics,[21,55] the rate constant of the binding reaction can be expressed as a difference of the rate constant of summative reaction, $k_{aqua+bind}$ and k_{aqua}: $k_{bind} = 2k_{aqua+bind} - k_{aqua}$. Note that the minimum interval between each pair of kinetic points that can be acquired by the present CZE method is about 15 min, approximated as the time spent for a CZE run and the capillary conditioning before injection of the next sample (both components could not be reduced without sacrificing the quality of separations).

Mass Spectrometry. An esquire3000 ion trap mass spectrometer (Bruker Daltonics, Bremen, Germany), equipped with an orthogonal ESI ion source, was used for MS measurements. For analyses of the intact complexes, the instrument was operated in negative ion mode, while positive ion mode was employed in experiments with proteins and protein−metal adducts. To ensure the best performance and to simulate physiological pH, samples containing varying drug-

to-protein ratios (from 1:1 to 10:1) were incubated at 37 °C in 20 mM ammonium bicarbonate buffer adjusted to pH 7.4 by titration with 0.1 M formic acid. The samples were measured twice after incubation periods of 30 and 180 min to ensure the equilibrium conditions. The solutions were introduced via flow injection at a rate of 4 μL/min using a Cole-Parmer 74900 single-syringe infusion pump (Vernon Hills, IL). The ESI-MS instrument was controlled by means of the esquireControl software (version 5.2), and all data were processed using DataAnalysis software (version 3.2) (both Bruker Daltonics).

Cell Lines and Culture Conditions. Human HT-29 (colon carcinoma) and SK-BR-3 (mammary carcinoma) cells were kindly provided by Prof. Brigitte Marian (Institute of Cancer Research, Medical University of Vienna, Austria) and Ms. Evelyn Dittrich (General Hospital, Medical University of Vienna, Austria), respectively. Cells were grown in 75 cm^2 culture flasks (Iwaki/Asahi Technoglass, Gyouda, Japan) as adherent monolayer cultures in complete culture medium, i.e., minimal essential medium (MEM) supplemented with 10% heat-inactivated fetal bovine serum, 1 mM sodium pyruvate, 4 mM L-glutamine, and 1% non-essential amino acids (100×) (all purchased from Gibco/Invitrogen, Paisley, U.K.). Cultures were maintained at 37 °C in a humidified atmosphere containing 5% CO_2.

Cytotoxicity Tests in Cancer Cell Lines. Cytotoxicity was determined by means of a colorimetric microculture assay. HT-29 and SK-BR-3 cells were harvested from culture flasks by trypsinization and seeded into 96-well microculture plates (Iwaki/Asahi Technoglass, Gyouda, Japan). Cell densities of 5×10^3 (HT-29) and 4×10^3 cells/well (SK-BR-3) were chosen in order to ensure exponential growth throughout drug exposure. After a 24 h preincubation, cells were exposed for 96 h to solutions of the test compounds prepared in culture medium (200 μL/well). At the end of exposure, drug solutions were replaced by 100 μL/well RPMI1640 culture medium (supplemented with 10% heat-inactivated fetal bovine serum) plus 20 μL/well MTT solution in phosphate-buffered saline (5 mg/mL PBS). After incubation for 4 h, the medium/MTT mixtures were removed, and the formazan crystals formed by the mitochondrial dehydrogenase activity of vital cells were dissolved in 150 μL dmso per well. Optical densities at 550 nm were measured with a Tecan Spectra Classic microplate reader (Grödig, Austria), using a reference wavelength of 690 nm in order to correct for unspecific absorption. The quantity of vital cells was expressed in terms of *T*/*C* values by comparison to untreated control microcultures, and IC_{50} values were calculated from concentration−effect curves by interpolation. Evaluation is based on means from at least three independent experiments, each comprising six microcultures per concentration level.

Acknowledgment. The authors are indebted to the FFG−Austrian Research Promotion Agency (Grant 811591), the Austrian Council for Research and Technology Development (Grant IS526001), the FWF−Austrian Science Fund (Grants P16186-NO3, P18123-N11, P16192-NO3, and P16498-N10), and COST D20. We are also thankful to Prof. Gerald Giester for X-ray data collection.

Supporting Information Available: X-ray crystallographic CIF files for (Ph_3PCH_2Ph)[*trans*-$RuCl_4$(atrz)(dmso-*S*)]·H_2O and (Ph_3PCH_2Ph)[*trans*-$RuCl_4$(dmso-*S*)(mtrz)], details for the crystal structure as well as the synthesis of compounds **4a**·H_2O and **5a**, ESI-MS measurement parameters, and elemental analysis data. This material is available free of charge via the Internet at http://pubs.acs.org.

References

(1) Alessio, E.; Mestroni, G.; Bergamo, A.; Sava, G. Ruthenium antimetastatic agents. *Curr. Top. Med. Chem.* **2004**, *4*, 1525−1535.
(2) Hartinger, C. G.; Zorbas-Seifried, S.; Jakupec, M. A.; Kynast, B.; Zorbas, H.; Keppler, B. K. From bench to bedside−Preclinical and early clinical development of the anticancer agent indazolium *trans*-[tetrachlorobis(1*H*-indazole)ruthenate(III)] (KP1019 or FFC14A). *J. Inorg. Biochem.* **2006**, *100*, 891−904.
(3) Rademaker-Lakhai, J. M.; van den Bongard, D.; Pluim, D.; Beijnen, J. H.; Schellens, J. H. A phase I and pharmacological study with imidazolium-*trans*-DMSO-imidazole-tetrachlororuthenate, a novel ruthenium anticancer agent. *Clin. Cancer Res.* **2004**, *10*, 3717−3727.
(4) Dittrich, C.; Scheulen, M. E.; Jaehde, U.; Kynast, B.; Gneist, M.; Richly, H.; Schaad, S.; Arion, V. B.; Keppler, B. K. Phase I and pharmacokinetic study of sodium *trans*-[tetrachlorobis(1*H*-indazole)-ruthenate(III)]/indazole hydrochloride (1:1.1) (FFC14A, KP1019) in patients with solid tumors−A study of the CESAR Central European Society for Anticancer Drug Research. *Proc. Am. Assoc. Cancer Res.* **2005**, *46*, P472.
(5) Ang, W. H.; Dyson, P. J. Classical and non-classical ruthenium-based anticancer drugs: Towards targeted chemotherapy. *Eur. J. Inorg. Chem.* **2006**, 4003−4018.
(6) Clarke, M. J. Ruthenium metallopharmaceuticals. *Coord. Chem. Rev.* **2003**, *236*, 209−233.
(7) Reisner, E.; Arion, V. B.; Guedes da Silva, M. F. C.; Lichtenecker, R.; Eichinger, A.; Keppler, B. K.; Kukushkin, V. Y.; Pombeiro, A. J. Tuning of redox potentials for the design of ruthenium anticancer drugs−An electrochemical study of [*trans*-$RuCl_4L(DMSO)]^-$ and [*trans*-$RuCl_4L_2]^-$ complexes, where L = imidazole, 1,2,4-triazole, indazole. *Inorg. Chem.* **2004**, *43*, 7083−7093.
(8) Ravera, M.; Baracco, S.; Cassino, C.; Zanello, P.; Osella, D. Appraisal of the redox behaviour of the antimetastatic ruthenium(III) complex [ImH][$RuCl_4$(DMSO)(Im)], NAMI-A. *Dalton Trans.* **2004**, 2347−2351.
(9) Schluga, P.; Hartinger, C. G.; Egger, A.; Reisner, E.; Galanski, M.; Jakupec, M. A.; Keppler, B. K. Redox behavior of tumor-inhibiting ruthenium(III) complexes and effects of physiological reductants on their binding to GMP. *Dalton Trans.* **2006**, *14*, 1796−1802.
(10) Sava, G.; Bergamo, A.; Zorzet, S.; Gava, B.; Casarsa, C.; Cocchietto, M.; Furlani, A.; Scarcia, V.; Serli, B.; Iengo, E.; Alessio, E.; Mestroni, G. Influence of chemical stability on the activity of the antimetastasis ruthenium compound NAMI-A. *Eur. J. Cancer* **2002**, *38*, 427−435.
(11) Khalaila, I.; Bergamo, A.; Bussy, F.; Sava, G.; Dyson, P. J. The role of cisplatin and NAMI-A plasma-protein interactions in relation to combination therapy. *Int. J. Oncol.* **2006**, *29*, 261−268.
(12) Pluim, D.; van Waardenburg, R. C.; Beijnen, J. H.; Schellens, J. H. Cytotoxicity of the organic ruthenium anticancer drug NAMI-A is correlated with DNA binding in four different human tumor cell lines. *Cancer Chemother. Pharmacol.* **2004**, *54*, 71−78.
(13) Brabec, V.; Novakova, O. DNA binding mode of ruthenium complexes and relationship to tumor cell toxicity. *Drug Resist. Updates* **2006**, *9*, 111−122.
(14) Hartinger, C. G.; Timerbaev, A. R.; Keppler, B. K. Capillary electrophoresis in anti-cancer metallodrug research: Advances and future challenges. *Electrophoresis* **2003**, *24*, 2023−2037.
(15) Timerbaev, A. R.; Hartinger, C. G.; Keppler, B. K. Metallodrug research and analysis using capillary electrophoresis. *Trends Anal. Chem.* **2006**, *25*, 868−875.
(16) Timerbaev, A. R.; Hartinger, C. G.; Aleksenko, S. S.; Keppler, B. K. Interactions of antitumor metallodrugs with serum proteins: Advances in characterization using modern analytical methodology. *Chem. Rev.* **2006**, *106*, 2224−2248.
(17) Casini, A.; Gabbiani, C.; Mastrobuoni, G.; Messori, L.; Moneti, G.; Pieraccini, G. Exploring metallodrug-protein interactions by ESI mass spectrometry: The reaction of anticancer platinum drugs with horse heart cytochrome c. *ChemMedChem* **2006**, *1*, 413−417.
(18) Pongratz, M.; Schluga, P.; Jakupec, M. A.; Arion, V. B.; Hartinger, C. G.; Allmaier, G.; Keppler, B. K. Transferrin binding and transferrin-mediated cellular uptake of the ruthenium coordination compound KP1019, studied by means of AAS, ESI-MS and CD spectroscopy. *J. Anal. At. Spectrom.* **2004**, *19*, 46−51.
(19) Messori, L.; Gonzales Vilchez, F.; Vilaplana, R.; Piccioli, F.; Alessio, E.; Keppler, B. K. Binding of antitumor ruthenium(III) complexes to plasma proteins. *Met.-Based Drugs* **2000**, *7*, 335−342.
(20) Piccioli, F.; Sabatini, S.; Messori, L.; Orioli, P.; Hartinger, C. G.; Keppler, B. K. A comparative study of adduct formation between the anticancer ruthenium(III) compound HInd *trans*-[$RuCl_4(Ind)_2$] and serum proteins. *J. Inorg. Biochem.* **2004**, *98*, 1135−1142.
(21) Timerbaev, A. R.; Rudnev, A. V.; Semenova, O.; Hartinger, C. G.; Keppler, B. K. Comparative binding of antitumor indazolium [*trans*-tetrachlorobis(1*H*-indazole)ruthenate(III)] to serum transport proteins assayed by capillary zone electrophoresis. *Anal. Biochem.* **2005**, *341*, 326−333.
(22) Gomme, P. T.; McCann, K. B.; Bertolini, J. Transferrin: Structure, function and potential therapeutic actions. *Drug Discovery Today* **2005**, *10*, 267−273.

(23) Reisner, E.; Arion, V. B.; Hartinger, C. G.; Jakupec, M. A.; Pombeiro, A. J. L.; Keppler, B. K. From synthesis to antitumor activity—NAMI-A and KP1019, two ruthenium complexes in clinical trials. In *Education in Advanced Chemistry, Perspectives of Coordination Chemistry*; Trzeciak, A. M., Ed.; Wydawnictwo Uniwersytetu Wrocławskiego: Poznan-Wrocław, 2005; Vol. 9, pp 215−229.
(24) Polec-Pawlak, K.; Abramski, J. K.; Semenova, O.; Hartinger, C. G.; Timerbaev, A. R.; Keppler, B. K.; Jarosz, M. Platinum group metallodrug-protein binding studies by capillary electrophoresis-inductively coupled plasma-mass spectrometry: A further insight into the reactivity of a novel antitumor ruthenium(III) complex toward human serum proteins. *Electrophoresis* **2006**, *27*, 1128−1135.
(25) Bouma, M.; Nuijen, B.; Jansen, M. T.; Sava, G.; Bult, A.; Beijnen, J. H. Photostability profiles of the experimental antimetastatic ruthenium complex NAMI-A. *J. Pharm. Biomed. Anal.* **2002**, *30*, 1287−1296.
(26) Bouma, M.; Nuijen, B.; Jansen, M. T.; Sava, G.; Flaibani, A.; Bult, A.; Beijnen, J. H. A kinetic study of the chemical stability of the antimetastatic ruthenium complex NAMI-A. *Int. J. Pharm.* **2002**, *248*, 239−246.
(27) Alessio, E. Synthesis and reactivity of Ru-, Os-, Rh-, and Ir-halide-sulfoxide complexes. *Chem. Rev.* **2004**, *104*, 4203−4242.
(28) Bergamo, A.; Gagliardi, R.; Scarcia, V.; Furlani, A.; Alessio, E.; Mestroni, G.; Sava, G. In vitro cell cycle arrest, in vivo action on solid metastasizing tumors, and host toxicity of the antimetastatic drug NAMI-A and cisplatin. *J. Pharmacol. Exp. Ther.* **1999**, *289*, 559−564.
(29) Bergamo, A.; Zorzet, S.; Cocchietto, M.; Carotenuto, M. E.; Magnarin, M.; Sava, G. Tumour cell uptake G2-M accumulation and cytotoxicity of NAMI-A on TS/A adenocarcinoma cells. *Anticancer Res.* **2001**, *21*, 1893−1898.
(30) Vacca, A.; Bruno, M.; Boccarelli, A.; Coluccia, M.; Ribatti, D.; Bergamo, A.; Garbisa, S.; Sartor, L.; Sava, G. Inhibition of endothelial cell functions and of angiogenesis by the metastasis inhibitor NAMI-A. *Br. J. Cancer* **2002**, *86*, 993−998.
(31) Zorzet, S.; Bergamo, A.; Cocchietto, M.; Sorc, A.; Gava, B.; Alessio, E.; Iengo, E.; Sava, G. Lack of in vitro cytotoxicity, associated to increased G(2)-M cell fraction and inhibition of matrigel invasion, may predict in vivo-selective antimetastasis activity of ruthenium complexes. *J. Pharmacol. Exp. Ther.* **2000**, *295*, 927−933.
(32) Pacor, S.; Zorzet, S.; Cocchietto, M.; Bacac, M.; Vadori, M.; Turrin, C.; Gava, B.; Castellarin, A.; Sava, G. Intratumoral NAMI-A treatment triggers metastasis reduction, which correlates to CD44 regulation and tumor infiltrating lymphocyte recruitment. *J. Pharmacol. Exp. Ther.* **2004**, *310*, 737−744.
(33) Casarsa, C.; Mischis, M. T.; Sava, G. TGFbeta1 regulation and collagen-release-independent connective tissue re-modelling by the ruthenium complex NAMI-A in solid tumours. *J. Inorg. Biochem.* **2004**, *98*, 1648−1654.
(34) Bouma, M.; Nuijen, B.; Jansen, M. T.; Sava, G.; Picotti, F.; Flaibani, A.; Bult, A.; Beijnen, J. H. Development of a LC method for pharmaceutical quality control of the antimetastatic ruthenium complex NAMI-A. *J. Pharm. Biomed. Anal.* **2003**, *31*, 215−228.
(35) Bacac, M.; Hotze, A. C.; van der Schilden, K.; Haasnoot, J. G.; Pacor, S.; Alessio, E.; Sava, G.; Reedijk, J. The hydrolysis of the anti-cancer ruthenium complex NAMI-A affects its DNA binding and anti-metastatic activity: An NMR evaluation. *J. Inorg. Biochem.* **2004**, *98*, 402−412.
(36) Jaswal, J. S.; Rettig, S. J.; James, B. R. Ruthenium(III) complexes containing dimethyl sulfoxide or dimethyl sulfide ligands, and a new route to *trans*-dichlorotetrakis(dimethyl sulfoxide)ruthenium(II). *Can. J. Chem.* **1990**, *68*, 1808−1817.
(37) Arion, V. B.; Reisner, E.; Fremuth, M.; Jakupec, M. A.; Keppler, B. K.; Kukushkin, V. Y.; Pombeiro, A. J. Synthesis X-ray diffraction structures, spectroscopic properties, and in vitro antitumor activity of isomeric (1*H*-1,2,4-triazole)Ru(III) complexes. *Inorg. Chem.* **2003**, *42*, 6024−6031.
(38) Haasnoot, J. G. Mononuclear, oligonuclear and polynuclear metal coordination compounds with 1,2,4-triazole derivatives as ligands. *Coord. Chem. Rev.* **2000**, *200−202*, 131−185.
(39) Turel, I.; Pecanac, M.; Golobic, A.; Alessio, E.; Serli, B.; Bergamo, A.; Sava, G. Solution solid state and biological characterization of ruthenium(III)-DMSO complexes with purine base derivatives. *J. Inorg. Biochem.* **2004**, *98*, 393−401.
(40) Velders, A. H.; Bergamo, A.; Alessio, E.; Zangrando, E.; Haasnoot, J. G.; Casarsa, C.; Cocchietto, M.; Zorzet, S.; Sava, G. Synthesis and chemical-pharmacological characterization of the antimetastatic NAMI-A-type Ru(III) complexes (Hdmtp)[*trans*-$RuCl_4$(dmso-*S*)(dmtp)], (Na)[*trans*-$RuCl_4$(dmso-S)(dmtp)], and [*mer*-$RuCl_3(H_2O)$(dmso-*S*)(dmtp)] (dmtp = 5,7-dimethyl[1,2,4]triazolo[1,5-*a*]pyrimidine). *J. Med. Chem.* **2004**, *47*, 1110−1121.
(41) Schafer, F. Q.; Buettner, G. R. Redox environment of the cell as viewed through the redox state of the glutathione disulfide/glutathione couple. *Free Radical Biol. Med.* **2001**, *30*, 1191−1212.
(42) Miklavcic, D.; Sersa, G.; Novakovic, S.; Rebersek, S. Tumor bioelectric potential and its possible exploitation for tumor growth retardation. *J. Bioelectr.* **1990**, *9*, 133−149.
(43) Huang, Z.; Timerbaev, A. R.; Keppler, B. K.; Hirokawa, T. Determination of cisplatin and its hydrolytic metabolite in human serum by capillary electrophoresis techniques. *J. Chromatogr., A* **2006**, *1106*, 75−79.
(44) Guideline on Impurities in New Drug Substances, International Conference on Harmonization; *Federal Register*; Government Printing Office: Washington, DC, 1996; p 372.
(45) Davies, J. A.; Hockensmith, C. M.; Kukushkin, V. Y.; Kukushkin, Y. N. *Synthetic Coordination Chemistry: Principles and Practice*; World Scientific: Singapore, 1996.
(46) Mura, P.; Piccioli, F.; Gabbiani, C.; Camalli, M.; Messori, L. Structure−function relationships within Keppler-type antitumor ruthenium(III) complexes: The case of 2-aminothiazolium [*trans*-tetrachlorobis(2-aminothiazole)ruthenate(III)]. *Inorg. Chem.* **2005**, *44*, 4897−4899.
(47) Gallori, E.; Vettori, C.; Alessio, E.; Vilchez, F. G.; Vilaplana, R.; Orioli, P.; Casini, A.; Messori, L. DNA as a possible target for antitumor ruthenium(III) complexes. *Arch. Biochem. Biophys.* **2000**, *376*, 156−162.
(48) Hartinger, C. G.; Ferri-Mendoza, M. G.; Nazarov, A. A.; Keppler, B. K. Electrospray ionization mass spectrometric study on the coordination behavior of dacarbazine towards transition metal ions. *Polyhedron* **2006**, *25*, 1971−1978.
(49) Shepherd, R. E.; Slocik, J. M.; Stringfield, T. W.; Somayajula, K. V.; Amoscato, A. A. Electrospray mass spectrometry of *cis*-[Ru(NO)Cl(bpy)$_2$]$^{2+}$ (bpy = 2,2′-bipyridine): Fragmentation from desolvated {[Ru(NO)Cl(bpy)2]$^{2+}$, Cl^-}$^+$ ion pairs by electron transfer and internal Lewis base pathways. *Inorg. Chim. Acta* **2004**, *357*, 965−979.
(50) Feng, R.; Konishi, Y.; Bell, A. W. High accuracy molecular weight determination and variation characterization of proteins up to 80 ku by ionspray mass spectrometry. *J. Am. Soc. Mass Spectrom.* **1991**, *2*, 387−401.
(51) Ravera, M.; Baracco, S.; Cassino, C.; Colangelo, D.; Bagni, G.; Sava, G.; Osella, D. Electrochemical measurements confirm the preferential bonding of the antimetastatic complex [ImH][$RuCl_4$(DMSO)(Im)] (NAMI-A) with proteins and the weak interaction with nucleobases. *J. Inorg. Biochem.* **2004**, *98*, 984−990.
(52) Seelig, M. H.; Berger, M. R.; Keppler, B. K. Antineoplastic activity of three ruthenium derivatives against chemically induced colorectal carcinoma in rats. *J. Cancer Res. Clin. Oncol.* **1992**, *118*, 195−200.
(53) *ExPASy Proteomics Server*; Swiss Institute of Bioinformatics: Basel, Switzerland, 2003; http://www.expasy.org/.
(54) Mestroni, G.; Alessio, E.; Sava, G. New salts of anionic complexes of Ru(III), as antimetastatic and antineoplastic agents. PCT Int. Appl. WO 98/00431, 1998.
(55) Sykes, A. G. *Kinetics of Inorganic Reactions*; Pergamon Press: London, 1966.
(56) Catalan, J.; Abboud, J. L. M.; Elguero, J., Basicity and acidity of azoles. In *Advances in Heterocyclic Chemistry*; Katritzky, A. R., Ed.; Academic Press: New York, 1987; Vol. 41.

JM061081Y